The rate of information transfer at graded-potential synapses

R. R. de Ruyter van Steveninck*† & S. B. Laughlin†

* NEC Research Institute, 4 Independence Way, Princeton, New Jersey 08540, USA
† Department of Zoology, University of Cambridge, Downing Street, Cambridge CB2 3EJ, UK

THERE are few estimates of the rates at which spiking neurons transmit information[1–5], and none for synapses transmitting graded signals. We have measured the rates at which blowfly (*Calliphora vicina*) photoreceptors transmit information through chemical synapses to large monopolar cells (LMCs). The graded responses of these non-spiking cells transmit as much as 1,650 bits per second, five times the highest rates measured in spiking neurons[3]. The widespread occurrence of non-spiking neurons in sensory systems could well reflect this superior performance. Comparing transmission rates in pre- and post-synaptic cells, we estimate that each synaptic active zone transmits ~50 bits s^{-1}. This estimate assumes statistical independence of the noise generated at active zones and makes use of a detailed morphometric analysis of photoreceptor–LMC synapses[6,7]. These measurements provide a benchmark for quantifying the performance of synaptic mechanisms and for understanding the limitations that synaptic transmission and spike coding place upon neural computation.

Information capacity is a basic measure, specifying the logarithm of the number of distinct messages that a signalling system can transmit per unit time. To estimate the information capacities of neurons, we must measure the reliability and dynamics of the neural code[1–5]. Photoreceptors of the fly compound eye code small intensity fluctuations as analogue changes in membrane potential. These graded potentials drive synapses that generate graded responses in the second-order neurons, the LMCs. For the functionally appropriate signals used here, signal and noise are approximately gaussian. For these conditions, Shannon[8] derived R, the rate of information transmission in bits s^{-1}, as

$$R = \int_0^\infty df \log_2\left[1 + \frac{S(f)}{N(f)}\right] \quad (1)$$

where $S(f)$ and $N(f)$ are the power spectral densities of signal and noise respectively. Note that this formulation considers both reliability and dynamics by treating the signal-to-noise ratio in the frequency domain.

Coding by photoreceptors and LMCs is approximately linear[9–11], enabling us to measure signal and noise spectral densities by recording graded-potential responses to a pseudorandom sequence of light intensity fluctuations. Here we specify this stimulus by the contrast modulation $c(t)$ (Fig. 1). The encoded signal is the average response, $v_{av}(t)$, to repeated presentations of $c(t)$. Note that stimulus and response are continuous functions of time, not single numbers. Each response to a single presentation deviates from the average, and from these random deviations we obtain the noise power spectral density $N(f)$ (Fig. 1).

Because coding is linear, it is described by a transfer function $T(f)$, which here is the contrast to voltage gain at each frequency.

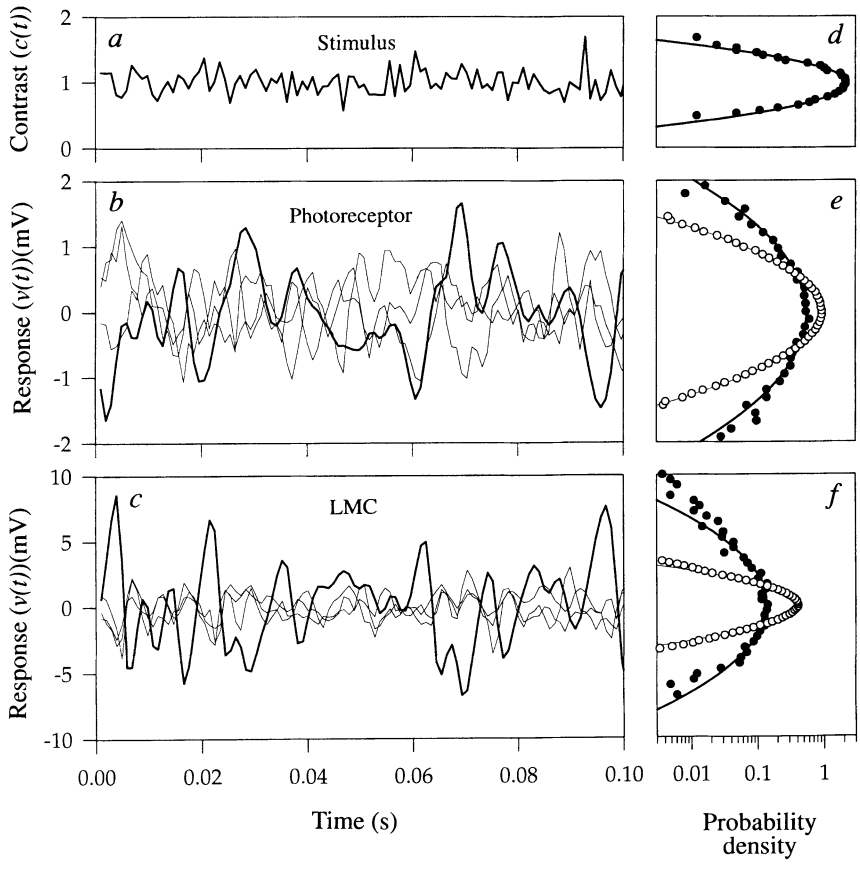

FIG. 1 Examples of raw data traces of the stimulus contrast signal (*a*), and the average voltages as well as the fluctuations around the average recorded from a photoreceptor (*b*) and an LMC (*c*). *d*–*f*, Probability distributions corresponding to these signals. Intracellular recordings were made from photoreceptors and LMCs in the retinae of intact blowflies, *Calliphora vicina*, using conventional microelectrode recording techniques[19]. All experiments were done at room temperature, 22–24 °C. The stimulus source was a high-intensity green LED modulated by a 2-s pseudorandom contrast sequence. Here we define contrast as $c(t) = I(t)/I_0$, with $I(t)$ the light intensity as a function of time, and I_0 its time-average; thus $c(t)$ is dimensionless with a time average of 1. This sequence, a short segment of which is shown in *a*, was repeated 76 times while an on-line computer recorded the set of cell voltage responses $\{v_i(t)\}$. The ensemble average of this set, $v_{av}(t)$ (thick lines in *b* and *c*), approximates the cell's noiseless response to $c(t)$. Subtracting $v_{av}(t)$ from each of the 76 voltage records gave the set of noise traces $[v_i(t) - v_{av}(t)]$, and averaging the power spectra of these traces gave the overall noise power density spectrum $N(f)$. Three representative noise traces are shown by the thin lines in *b* and *c*. In most cases, as in this example, the modulated stimulus $c(t)$ had a gaussian distribution (data points and gaussian fit are shown in *d*) with a flat contrast power density of $\sim 3.1 \times 10^{-5}$ Hz^{-1} up to 500 Hz. As expected[9–11], photoreceptors responded linearly to this stimulus, producing a gaussian distribution of signal levels (filled circles in *e*) and of noise (open circles in *e*). Gaussian fits to the data points are shown as the continuous lines. LMC linearity was checked explicitly by recording responses to two different contrast waveforms and to their superposition. The response to the summed stimulus was very close to the sum of the responses to the individual random waveforms, as required for linearity. The distributions of LMC signal (filled circles in *f*) and noise (open circles in *f*) deviated somewhat from gaussian (continuous lines). However, for computing the information rate, the approximation is still quite reasonable. This was checked by comparing the entropy difference between the measured signal and noise distributions (2.81 bits) to the entropy difference between the fitted signal and noise distributions (3.03 bits). With these conditions, equation (1) gives a good approximation to the information transmission of the cells.

$T(f)$ is determined directly as the ratio of the frequency components of the measured average voltage signal and the stimulus contrast: $T(f) = V_{av}(f)/S_C(f)$, where $V_{av}(f)$ and $S_C(f)$ are the Fourier transforms of $v_{av}(t)$ and $c(t)$. To combine data from different cells, we use a common measure appropriate for both photoreceptors and LMCs, namely the power spectral density of equivalent contrast noise, $N_C(f)$ (Fig. 2). This is defined as a stimulus contrast power spectral density that, after filtering by $T(f)$, would have the same spectral density as the measured noise: $N_C(f) = N(f)/|T(f)|^2$.

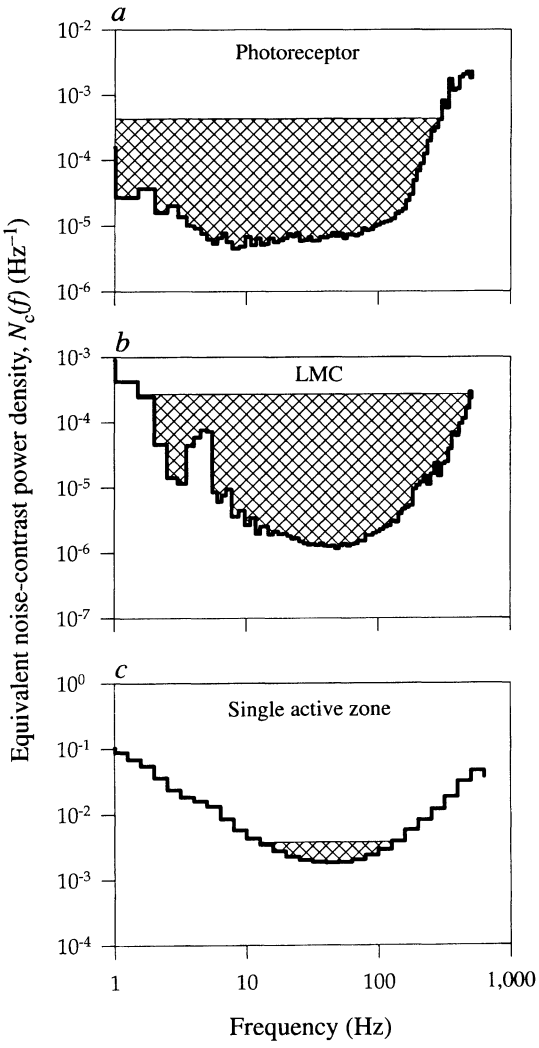

FIG. 2 An account of the procedure used to measure information transfer rates and information capacities. Equivalent contrast noise spectral densities (thick lines), and distribution of optimal stimulus contrast spectral density (cross-hatched areas) for a photoreceptor (*a*), an LMC (*b*), and a single synaptic active zone (*c*). Note the differences in vertical scales, and in particular that the total surface area in the cross-hatched areas in all three panels is equal to 0.1. Shannon[8] considered the problem of optimal signal transmission through a gaussian channel, given that the total transmitted power is limited. Our problem is the same, except that we fix the total signal power, that is, we fix the stimulus contrast spectral density integrated over frequency. The solution[8] of the optimization problem is to distribute the contrast power over the different frequency bands in such a way that the summed contribution of signal plus noise power densities is flat where that is possible. This is analogous to filling a vessel shaped as the equivalent contrast noise spectrum with an amount of water that is representative of the total stimulus contrast power. This filling was performed by an iterative procedure, with a fixed total contrast power of 0.1. From the resulting contrast power spectral density, $S_c(f)$, we then derive the information capacity by equation (1). The equivalent contrast power spectral density shown in *c* is based on interpolated experiment data (Fig. 4). This particular example was computed for the same bump rate as the data shown in *b*. Note that here we compute the information capacity for the transfer of contrast information. This is not quite the same as the information capacity for transfer of pre- to postsynaptic voltage. The error is very small, as the spectra are quite flat in the region of interest; moreover, the error will lead to an underestimate of the true value.

The information transmission rate R now follows from substituting $N_C(f)$ and $S_C(f)$ into equation (1). However, R depends not only upon system performance, as measured by $N_C(f)$, but upon one's choice of signal, $S_C(f)$. A more universal measure is the information capacity, R_{max}, defined as the maximum transmission rate, achieved by selecting the stimulus $S_C(f)$ that optimally drives the cell. Because R_{max} is increased by boosting stimulus contrast, the contrast variance of $S_C(f)$ was fixed at 0.1. This is a natural choice, as it is representative of natural levels[12,13] and falls within the linear response range of photoreceptors and LMCs. Having fixed the total contrast, we derive $S_C(f)$ for the optimum stimulus (Fig. 2), and use this to calculate the information capacity R_{max} (equation (1)).

Data from five photoreceptors and three LMCs produce consistent estimates of information capacity (Fig. 3). Information capacities rise steadily with mean intensity, as expected of a system partly limited by photon shot noise. LMCs demonstrate the benefits of the convergence of signals from six photoreceptors[14–16], achieving a capacity of 1,650 bits s^{-1}, as compared with 1,000 bits s^{-1} in photoreceptors. Note that, because of the redundancy inherent to parallel transmission of the same signal, the postsynaptic information capacity is far less than the sum of the presynaptic capacities.

The synaptic information capacity can be deduced by comparing the pre- and postsynaptic equivalent noise spectral densities, $N_{Cpre}(f)$ and $N_{Cpost}(f)$. The comparison must be between cells

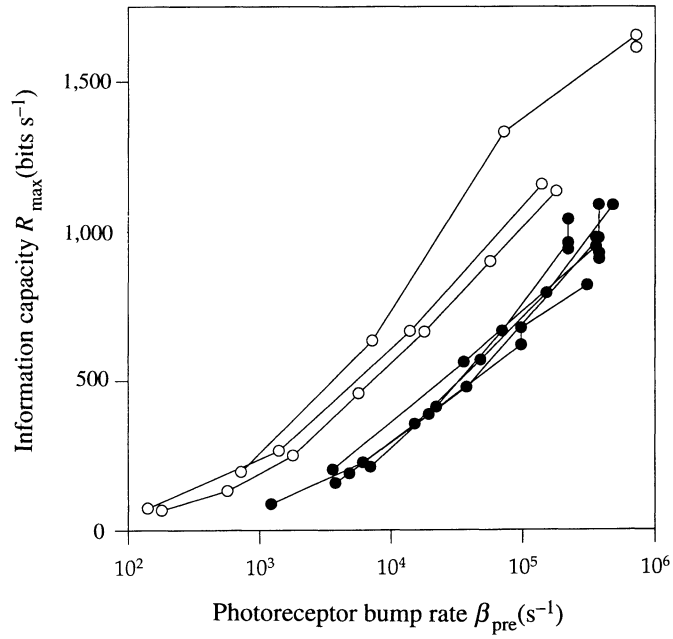

FIG. 3 Information capacities of photoreceptors and LMCs as a function of mean light intensity, computed according to equation (1), with an optimal contrast stimulus as defined in the legend to Fig. 2. Light intensity along the abscissa is expressed as the number of photoconversions per photoreceptor per second. This measure of effective intensity was extrapolated from counts of quantum bumps (electrical events triggered by single photon absorptions[17]) at low light levels and the values of the calibrated neutral density filters used to attenuate the light source. The bump rate measured in LMCs was divided by 6 to give the bump rate in each of the 6 pre-synaptic photoreceptors. Lines connect points belonging to an individual cell. The high information rates assume an optimal stimulus but are not unreasonable: with non-optimized but stronger stimuli (total contrast power, 0.28), we directly measured LMC transinformation rates of 1,150 bits s^{-1}.

driven by stimuli of equivalent quantal content, because bit rates depend on photon flux (Fig. 3). Strict equivalence could not be achieved by recording simultaneously from a photoreceptor and its postsynaptic LMC. Instead we calibrated the quantum catch of each recorded cell and corrected for the small differences. Calibration was done by counting the rate of production of quantum bumps, discrete voltage pulses produced at very low light levels by single photon hits[17–19]. When intensity was increased in calibrated steps, the low-level count was increased by the same factor to give the extrapolated bump rate, β. From measurements of $N_C(f)$ made at different values of β, we interpolate to derive $N_C(f, \beta)$, the function that specifies the equivalent contrast noise spectrum for different β values (Fig. 4).

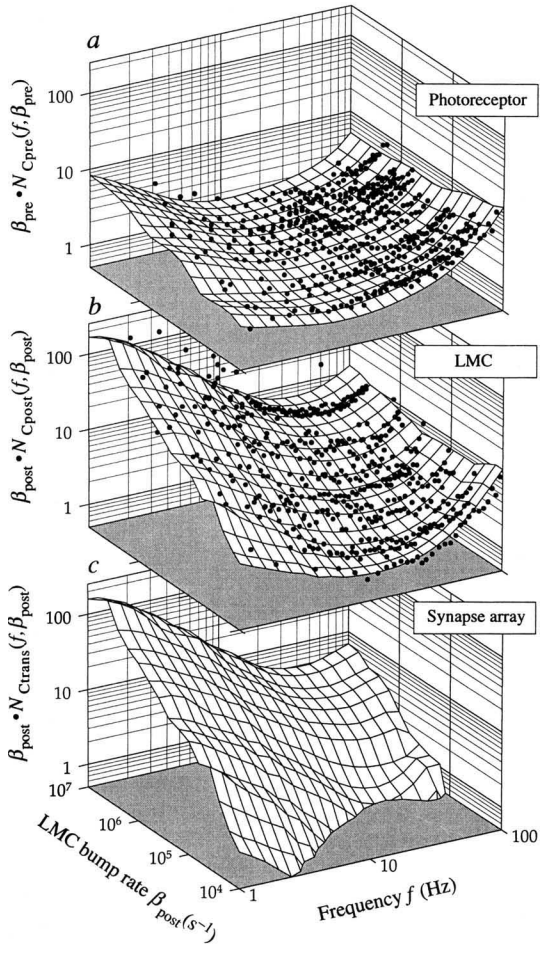

FIG. 4 *a*, *b*, Measured values (black dots) of $\beta \cdot N_C(f, \beta)$ for three photoreceptors (*a*) and three LMCs (*b*), together with smooth surfaces obtained from interpolation of the data points. The values of β specified on the left-hand axes are the postsynaptic LMC bump rate β_{post}. The presynaptic rate is $\beta_{pre} = \beta_{post}/6$. Equivalent contrast power spectral densities for each value of β are computed as $N_C(f, \beta) = N(f, \beta)/|T(f, \beta)|^2$. Shot noise analysis shows that, owing to photon poisson statistics, an ideal photon counter absorbing photons at the extrapolated bump rate should have $\beta \cdot N_C(f, \beta) = 1$. A realistic photon counter then obeys $\beta \cdot N_C(f, \beta) \geq 1$, or in other words, $(\beta \cdot N_C(f, \beta))^{-1}$ is a measure of the detector's quantum efficiency. For the photoreceptors and LMCs studied here, this must be interpreted as a measure of efficiency relative to the dark-adapted state, in which the bump count was calibrated. From about 5 to 50 Hz, the photoreceptor's performance is within a factor of two from the ideal behaviour. At its best frequency, the LMC stays within a factor of 7 from the limit of 10^7 s^{-1} set by the bump rate. For both cells, the efficiency decreases at high frequencies, presumably as a result of time jitter in the transduction process. The decrease in efficiency at low frequencies results at least partly from instrumental noise. The interpolated surfaces give a fair representation of the measured data for each cell type, indicating that $N_C(f, \beta)$ is a good universal description of the behaviour of each cell type. c, The equivalent contrast noise contribution of the full synaptic array. The figure shows $\beta \cdot N_{Ctrans}(f, \beta)$ (see equation (3)), which is computed by subtracting the surface in *a* from that in *b*. $\beta \cdot N_{Ctrans}(f, \beta)$ must be interpreted as the contribution of synaptic transmission noise relative to the photon shot noise. At low values of β, we see that $\beta \cdot N_{Ctrans}(f, \beta) \ll 1$, so photon noise dominates the synaptic noise. Values below 0.5 are not shown, as low values are hard to estimate reliably. At higher intensities, $\beta \cdot N_{Ctrans}(f, \beta)$ increases, indicating that synaptic transmission, rather than the photon flux, becomes the information bottleneck[19].

We calculate synaptic transmission rates as follows. Six photoreceptors carrying identical signals converge upon a single LMC and contribute equally to the postsynaptic response[6,16]. Thus, when transmitting the same signal, the bump rate in a photoreceptor is one sixth that in an LMC: $\beta_{pre} = \beta_{post}/6$. The six photoreceptors contribute independent noise so that convergence improves the signal-to-noise ratio, reducing the equivalent contrast power of presynaptic noise by a factor of 6. Given that the total postsynaptic noise is the sum of noise injected by photoreceptors and noise introduced during transmission, $N_{Ctrans}(f, \beta)$, we have:

$$N_{Cpost}(f, \beta_{post}) = \frac{N_{Cpre}(f, \beta_{pre})}{6} + N_{Ctrans}(f, \beta_{post}) \qquad (2)$$

Calculating $N_{Ctrans}(f, \beta)$ from equation (2), we obtain a synaptic information capacity of 2,110 bits s^{-1} at our highest light intensity. This synaptic rate exceeds the LMC rate of 1,650 bits s^{-1} because it is equivalent to the capacity of an LMC that is driven by noise free photoreceptors.

Photoreceptor–LMC synapses resemble their graded response counterparts in the vertebrate retina in several respects. Their active zones, measuring $0.5 \times 0.2\,\mu m$, contain a high density of vesicles grouped around a prominent presynaptic structure[7]. Each active zone faces a tetrad of postsynaptic elements in which the dendrites of two LMCs form the central pair. In the housefly *Musca* each of the six presynaptic photoreceptors drives an LMC with approximately 200 separate and regularly spaced active zones, giving a total of approximately 1,200 zones driving each LMC[6]. With an optimal synaptic coding strategy, every zone would carry a unique signal component, at a rate of $2,110/1,200 = 1.8$ bits s^{-1}. However, this strategy requires sophisticated encoding mechanisms (for example, tuning individual zones to a personalized narrow band of signal frequencies or decorrelation through local spatial interactions) for which there are no precedents in graded synapses. Indeed, the active zones are structurally identical[6,7], and appear to act in parallel to induce additive postsynaptic responses, with approximately linear transmission from photoreceptor to LMC[16,19,20]. Thus the available evidence suggests that this array of active zones is employed to average out synaptic noise[21], leading to considerable redundancy because each zone carries, on average, the same signal. With m zones in parallel, the synaptic response amplitude and the total synaptic noise power both increase by a factor of m. Consequently, for the full array

$$N_{Ctrans}(f) = \frac{m \cdot N_{zone}(f)}{[m \cdot |T_{zone}(f)|]^2} = \frac{N_{zone}(f)}{m \cdot |T_{zone}(f)|^2} = \frac{N_{Czone}(f)}{m} \qquad (3)$$

with $N_{Czone}(f)$ the equivalent contrast spectral density of a single zone. Computing $N_{Czone}(f)$ from equations (2) and (3) at the highest β and combining this with an optimized stimulus of contrast variance 0.1 (Fig. 2), gives (equation (1)) an information capacity of 55 bits s^{-1} per active zone. Owing to redundancy, just as with converging photoreceptors, the total information capacity is far below the sum of the individual capacities. The number of zones is unknown for *Calliphora*, so that we have used data from the smaller fly *Musca*. However, any overestimate of active zone capacity will be small because the neurons of the two species are similar in size[22]. Moreover, the noise in each zone could be non-gaussian, in which case we underestimate the information capacity.

Our study demonstrates that sensory neurons and chemical synapses are remarkably effective. The information capacities of photoreceptors and LMCs are respectively 3 and 5 times higher

than the maximum rates reported by spiking neurons, measured in cricket cercal afferents[3]. This large difference implies that graded potential neurons are specialized for fast and accurate signalling over short distances[23,24], so explaining their widespread use in sensory systems[21]. Moreover, information can easily be lost when graded synaptic inputs are converted into spike trains and this, together with the information capacity of synapses, must constrain neural network design. Information capacities also set constraints upon the underlying molecular mechanisms. For example, the information capacity of a single active zone, about 50 bits s^{-1}, ultimately depends upon the precision of synaptic vesicle discharge. Any description of synaptic transmission that cannot account for this level of performance is incomplete. Thus measures of information capacity provide benchmarks for understanding the performance and design of neural systems at the network, cellular and molecular levels. □

Received 28 July; accepted 30 November 1995.

1. Eckhorn, R. & Pöpel, B. *Biol Cybern.* **17,** 7–17 (1975).
2. de Ruyter van Steveninck, R. & Bialek, W. *Proc. R. Soc. London.* B**234,** 379–414 (1988).
3. Warland, D., Landolfa, M., Miller, J. P. & Bialek, W., in *Neural Systems: Analysis and Modeling* (ed. Eeckman, F. H.) 327–333 (Kluwer Academic, Boston, 1993).
4. Bialek, W., Rieke, F., de Ruyter van Steveninck, R. & Warland, D. *Science* **252,** 1854–1857 (1991).
5. Kjaer, T., Hertz, J. & Richmond, B. J. *Compl. Neurosci.* **1,** 109–139 (1994).
6. Nicol, D. & Meinertzhagen, I. A. *J. comp. Neurol.* **207,** 29–44 (1982).
7. Fröhlich, A. *J. comp. Neurol.* **241,** 311–326 (1985).
8. Shannon, C. E. *Proceedings of the Institute of Radio Engineers* **37,** 10–21 (1949).
9. Leutscher-Hazelhoff, J. T. *J. Physiol.* **246,** 333–350 (1975).
10. French, A. S. & Järvilehto, M. *J. comp. Physiol.* **126,** 87–96 (1978).
11. Juusola, M., Uusitalo, R. O. & Weckström, M. *J. gen. Physiol.* **105,** 117–147 (1995).
12. Laughlin, S. B. *Z. Naturf.* **36**c 910–912 (1981).
13. Ruderman, D. & Bialek, W. *Phys. Rev. Lett.* **73,** 814–817 (1994).
14. Braitenberg, V. *Expl. Brain Res.* **3,** 271–298 (1967).
15. Kirschfeld, K. *Expl. Brain Res.* **3,** 248–270 (1967).
16. van Hateren, J. H. *J. comp. Physiol.* A**161,** 849–855 (1987).
17. Fuortes, M. G. F. & Yeandle, S. *J. gen. Physiol.* **47,** 443–463 (1964).
18. Howard, J., Blakeslee, B. & Laughlin, S. B. *Proc. R. Soc. Lond.* B **231,** 415–435 (1987).
19. Laughlin, S. B., Howard, J. & Blakeslee, B. *Proc. R. Soc. Lond.* B **231,** 437–467 (1987).
20. van Hateren, J. H. & Laughlin, S. B. *J. comp. Physiol.* A**166,** 437–448 (1990).
21. Laughlin, S. B. *J. comp. Physiol.* **84,** 335–355 (1973).
22. Strausfeld, N. J. *Atlas of an Insect Brain* (Springer, Berlin, 1976).
23. Pearson, K. G. in *Simpler Networks and Behaviour* (ed. Fentress, J. C.) 99–110 (Sinauer, Sunderland, 1976).
24. Bush, B. M. H. in *Neurones without Impulses* (eds Roberts, A. & Bush, B. M. H.) (Cambridge University Press, Cambridge, 1981).

ACKNOWLEDGEMENTS. We thank W. Bialek for suggestions, and I. Meinertzhagen, H. Barlow, D. Ruderman, D. O'Carroll, J. Anderson, P. Newland, D. Bray and R. Hardie for critical comments. R.d.R.v.S. was supported by a Royal Society Science Exchange Fellowship and S.B.L. by grants from the SERC Invertebrate Neuroscience Initiative, BBSRC & EPSRC Image Interpretation Initiative.

Inhibition of acute lymphoblastic leukaemia by a Jak-2 inhibitor

Naftaly Meydan*, Tom Grunberger*, Harjit Dadi*, Michal Shahar*, Enrico Arpaia*, Zvi Lapidot†, J. Steven Leeder*, Melvin Freedman*, Amos Cohen*, Aviv Gazit‡, Alexander Levitzki‡ & Chaim M. Roifman*§

* Divisions of Immunology/Allergy, Haematology and Pharmacology, The Hospital for Sick Children, and the Department of Pediatrics, University of Toronto, Toronto M5G 1X8, Canada
† Department of Immunology, The Weizmann Institute, Rehovot, Israel
‡ Department of Biological Chemistry, Institute of Life Sciences, The Hebrew University, Jerusalem, Israel

Acute lymphoblastic leukaemia (ALL) is the most common cancer of childhood. Despite the progress achieved in its treatment, 20% of cases relapse and no longer respond to chemotherapy. The most common phenotype of ALL cells share surface antigens with very early precursors of B cells and are therefore believed to originate from this lineage[1,3] Characterization of the growth requirement of ALL cells indicated that they were dependent on various cytokines, suggesting paracrine and/or autocrine growth regulation[4–6]. Because many cytokines induce tyrosine phosphorylation in lymphoid progenitor cells, and constitutive tyrosine phosphorylation is commonly observed in B-lineage leukaemias[7,8], attempts have been made to develop protein tyrosine kinase (PTK) blockers of leukaemia cell growth[9,10]. Here we show that leukaemic cells from patients in relapse have constitutively activated Jak-2 PTK. Inhibition of Jak-2 activity by a specific tyrosine kinase blocker, AG-490, selectively blocks leukaemic cell growth *in vitro* and *in vivo* by inducing programmed cell death, with no deleterious effect on normal haematopoiesis.

We analysed a large selection of tyrphostins as potential blockers of the growth of relapsed ALL cells. Among the tyrphostins tested (Fig. 1*a*), AG-490 was the most effective inhibitor of DNA synthesis in multiple ALL cell lines. The dose-dependent inhibition of DNA synthesis in G_2, A_1 and C_1 leukaemia cell lines is shown in Fig. 1*b*. At 5 μM AG-490, growth of all pre-B ALL cells was almost completely blocked. Other tyrphostins (Fig. 1*a*), such as the epidermal growth factor-receptor inhibitor quinazoline AG-1478 (ref. 11), AG-18 and AG-1007, HER-2/neu kinase inhibitor AG-879, and the B-cell antigen-receptor blockers AG-30 and AG-126 (ref. 12), had no inhibitory effect on DNA synthesis in ALL cells. Furthermore, AG-490 had no significant effect on the growth of mitogen-stimulated normal B or T cells, B-cell lymphoma (Ramos) or T-cell leukaemia (Molt-13) cells (Fig. 1*b*). The stringent structural requirement for growth inhibition by tyrphostins suggests that AG-490 has a specific effect on leukaemic cells as a result of inhibition of tyrosine kinase activity rather than nonspecific toxicity. Support for this hypothesis comes from the dose-dependent inhibition of tyrosine phosphorylation by AG-490 in all ALL cells tested (Fig. 2*a*). These results indicate that the tyrphostin AG-490 specifically inhibits the activity of a protein tyrosine kinase that is constitutively activated in all of the leukaemic cells tested.

Because many lymphokine receptors share common PTK signalling pathways[13–19], we examined the possibility that one (or more PTK could be linked to the uncontrolled growth of leukaemic cells. We therefore systematically assessed the identity of the cytoplasmic PTKs in leukaemic cells and their sensitivity to AG-490. We first examined the Jak family of kinases, which are associated with growth-factor receptors in haematopoietic and lymphoid cells[13–18]. This family has four members Jak-1, Jak-2, Jak-3 and Tyk-2, all of which possess two non-identical kinase domains and unique amino-terminal sequences[20–22]. Immunoprecipitation and subsequent blotting with antibodies raised against Jak-1, Jak-3 (Fig. 2*b*) and Jak-2 (Fig. 2*c*) shows that, in G_2 ALL, Jak-2 is abundantly expressed but Jak-1 and Jak-3 are below detection as compared with activated T cells. Furthermore, Jak-2 is tyrosine-phosphorylated in G_2 cells, (Fig. 2*d*) but not in normal pre-B cells (Fig. 2*e*), and its phosphorylation is inhibited by AG-490 in a dose-dependent manner, suggesting a constitutive activation in this kinase in ALL. Consistent with these results, *in vitro* kinase activity of Jak-2 was inhibited in a dose-dependent manner, whether AG-490 was added before (Fig. 2*f*, *g*) or during the reaction (data not shown). The AG-490 concentrations that block G_2 cell proliferation and Jak-2 activity *in vitro* (Fig. 2*f*) and in intact cells (Fig. 2*d*) are almost identical. *In vitro* kinase activities of Lck, Lyn, Btk, Syk, and Src, which are abundantly expressed in these cells[23,24], remained unaffected by AG-490 treatment (Fig. 2*h*). Identical results were obtained by treating whole cells with AG-490, or adding it directly to the kinase

§ To whom correspondence should be addressed.